

Influence of anodizing time on porosity of nanopore structures grown on flexible TLC aluminium films and analysis of images using MATLAB software

C. C. Vidyasagar^{1*}, Parashuram Bannigidad², H. B. Muralidhara³

¹Department of Chemistry, Rani Channamma University, Belgaum 591156, India

²Department of Computer science, Rani Channamma University, Belgaum 591156, India

³Centre for Emerging Technologies, Jain University, Bangalore 562112, India

*Corresponding author. E-mail: vidya.891@gmail.com

Received: 29 April 2015, Revised: 04 October 2015 and Accepted: 05 December 2015

ABSTRACT

The effect of time on nanopore structures formed via electrochemical anodization of high purity Al₂O₃ was investigated. The electrochemical bath consists of 5 % phosphoric acid electrolyte; a platinum electrode was used as the cathode electrode, and TLC (thin layer chromatography) aluminium film as anode electrode. It is found that the regularity of nanopores arrangement can be significantly improved by increasing anodizing time at constant temperature and voltage. It is observed after the anodizing process, that at every interval of time there is a significant decrease in wall thickness from 58-26nm and increase in the nanopore diameter size about 31-86 nm. According to Nielsch, self-ordering of porous alumina requires a porosity of 10 % independently of anodizing conditions. It means that the most optimum anodizing conditions always results in a porosity of 10 %. The result optimized at 30 min is well matched with 10 % porosity. The morphology and phase composition were characterized by field emission scanning electron microscope (FE-SEM), energy dispersive spectroscopy (EDX). The nanopores thin film images obtained by FESEM are used for image analysis using MATLAB software and porosity and nanowall thickness results are compared with experimental and automated methods, which demonstrate the efficacy of the proposed method. Copyright © 2016 VBRI Press.

Keywords: Anodization; computational chemistry; MATLAB; phosphoric acid; nanopores.

Introduction

The main requirement for any competitive photovoltaic (PV) technology is the cost per watt installed. To achieve this goal, a PV technology must not only have a low unit area cost, but also high efficiency. Nanopillar (NPL) and nanowire (NW) PV [1] address these requirements in three ways: (i) direct growth of crystalline materials on low cost substrates without the use of complex epitaxial processes, (ii) maximization of carrier collection efficiency by decoupling the light absorption and carrier collection directions, and (iii) minimization of optical losses by reduced reflection and enhanced absorption. Significant work has been carried out in recent years on all aspects of NPL photovoltaics including synthesis [2], optical properties [3- 6], and device physics [7-9]. Additionally, both single NW devices [10-11] and arrays [12-13] have been studied in detail. In the past decade, they have been extensively investigated as the building blocks for various technological applications such as electronics, optoelectronics [14, 15], and sensors [16].

Recently, as an emerging field, NWs have been utilized for energy harvesting devices, for instance, to convert thermal [17], mechanical [18], and solar energy into

electricity [19]. On the other hand, the NPL axial and radial junctions provide a three dimensional (3-D) geometric configuration for reduced surface optical reflection and enhanced absorption. The enhanced carrier collection and optical absorption can in principle enable more efficient PVs as compared to planar structures. However, the surface and the interface area enhancement also result in an increase in surface/interface recombination events. The ordering of the NPL arrays may be used as light trapping schemes analogous to random surface texturization or periodic grating couplers in thin films [20]. NW arrays can be used to redistribute the absorption spectrum from regions where absorption is not needed to spectral regions where absorption enhancement would lead to enhanced photocurrents. Each architecture has its advantages and drawbacks with respect to the control over optical properties and electronic properties as well as ease of fabrication. Embedded NPLs enable maximization of carrier collection by adjusting the NPL pitch, allowing moderate efficiencies to be achieved even if the absorber material has a low bulk minority carrier lifetime. On the other hand, free-standing core-shell NPLs, enable optical engineering of the structure by controlling the size and

pitch of the NPLs, as well as the possibility to tune the carrier collection by varying the core-shell radii. This method is more challenging to fabricate, as a conformal coating is needed to form a p-n junction. Manufacturing of well-ordered nanostructures on the length scales less than dozens nm by conventional optical lithography is a great challenge. Advanced non-optic lithography technique such as e-beam X-ray, and interference lithography is highly sufficient to be successfully employed for nanostructuring of materials in a scale of few nm, but required sophisticated facilities makes them unavailable to a lot of researchers.

Therefore a lot of alternative methods have been developed for the formation of nanopore and nanodot on various substrates including sol-gel method. In one example, to fabricate embedded CdS/CdTe NPL PV cells, a porous anodic aluminum oxide (AAO) was used as a template for nanomaterial growth [1, 21]. In short, a porous anodization of aluminium oxide (AAO) template is fabricated for subsequent NPL growth at the bottom of each pore. The AAO template is etched back, exposing the pillars, and the semiconductor absorber layer is then deposited. This process enables the fabrication of an NPL cell on a low-cost Al films. When anodized in an acidic environment with proper process conditions, aluminum oxidizes to form a pores alumina layer consisting of hexagonally packed arrays of nanopores [22], the pores are normal to the aluminum surface and extend from the surface to the alumina/aluminum interface where there is an oxide barrier layer with near hemispherical geometry. The shape and size of the pores are relatively uniform, with the pitch and diameter being directly proportional to the anodization voltage, and the height controlled by the anodization time. Anodized aluminumoxide (AAO) has proven to be a highly versatile material system that has found important applications in photonics, energy devices including supercapacitors, filtration and purification and architectural and anticorrosive finishes [23-25]. Furthermore, given the uniformity of size-controlled nanopores, AAO has been widely utilized as a template for ordered synthesis of nanostructured materials, including metallic and semiconductor nanorods [26, 27] nanowires [28, 29] nanotubes [30] and nanoparticles [31]. Importantly, aluminium anodization, in principle, is a highly scalable process as long as a stable voltage and current density are applied with a constant electrolyte temperature anodization time and composition. The protection or decoration of Al surfaces by anodization has been used commercially since at least 1923. Self-organized "nanopore" structures in anodic alumina films, called "alumite", have attracted great attention due to their high pore density and their potential use for masking or information storage. When the pores are filled with metals or semiconductors in a subsequent alternating-current reductive electrolysis, these films can be fabricated into interesting magnetic recording, electronic, and electro optical devices [29-31]. By considering these constraints, here demonstrated continuous change in pore diameter, wall thickness and porosity and inter pore distance as anodization time increases. The microscopic image analysis of nanoparticles by edge detection using ant colony optimization has been investigated by Shwetabh Singh [30]. The estimation of nanopores size distributions by image

analysis using deformable ellipse model was carried out by Fishker *et al.* [32, 33].

In this paper the anodic oxide formed on pure Al TLC film without any pre-anneal is investigated. The effects of anodizing time, concentration and temperature on the structural properties of the oxide films are examined in detail through digital image analysis. Automated microscopic image analysis provides an efficient tool for qualitative analysis in modern material science and biological studies. The main advantages of using digital image processing and pattern recognition techniques in conjunction with microscopy for quantitative studies of anodizing alumina; automatic image analysis reduces the amount of tedious work with microscopes needed to perform a more accurate quantitative analysis and these techniques provide an important quantitative tool to analyze the structures and spatial features of Al₂O₃ films.

Experimental

Materials and methods

TLC Silica Gel 60 F₂₅₄ plates were procured from Merck. Orthophosphoric acid was procured from s-d fine Chem. Ltd. Mumbai. Double distilled water was used throughout the experiments. DC power supply source-measure unit was used as the power supply to measure voltage or current simultaneously (Aplab: L6405). MATLAB version 7.9.0.529 (R2009) software, which was installed on PC (*hp*: G42, 2012) used for image analysis.

TLC plates were cut into proper size of 2x4 cm (0.5 mm thickness) of the following chemical composition (wt %) : Al 99.79 % (Aluminium), Cu 0.05 % (Copper), Mg 0.05 % (Magnesium), Si 0.05 % (Silicon), Mn 0.05 % (Manganese) and Zn 0.01 % (Zinc). *Coated silica was removed by rubbing* the surface using emery sheet grit 600. The Al plates were washed with distilled water, rinsed with ethanol, degreased with acetone in ultrasonic bath for 15 min. Finally the Al plates were purged by distilled water in ultrasonic bath for another 10 min. Before anodizing, the electrochemical polishing of samples was carried out in a 0.75 M NaOH solution. Al plates were immersed in NaOH solution for 4 min to remove alkaline impurities. The samples were rinsed with distilled water and acetone. Later onwards Al plates were rinsed thoroughly and kept undisturbed in distilled water for 10 min. Anodization was performed in a conventional cell using a platinum helical wire as a cathode. Al was used as the counter-electrode, and typically about 90 % of the Al was immersed in the electrolyte while the exposed one was connected to the anode through a crocodile clips. The working surface area of the sample was 1 cm². The back surface and the edges of the samples were insulated by an acid resistant paint layer. The electrical contact was made at the edge of the electrodes. Pt electrode served as the cathode electrode and the distance from the anode electrode was 3 cm. The samples were anodized in an acidic aqueous solution at different time interval at constant concentration and voltage. Ice cold water was used to maintain low temperatures using thermometer. During anodization the electrolyte was kept undisturbed, and the values of voltage, current, time and temperature were recorded. After the

anodization process, the samples were rinsed thrice in deionized water and acetone and dried at 90 °C for 1 hour in an oven and was wrapped in aluminium foil. The variation in the time could be attributed to change in the pore size and wall thickness of the anodized Al₂O₃ thin films.

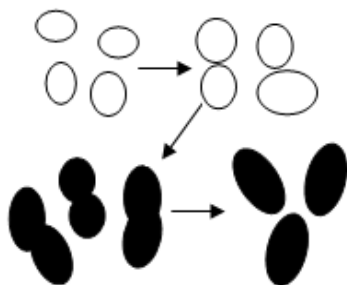
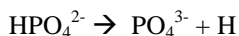


Fig. 1. Nucleation mechanism of pore.

Results and discussion

Mechanism of pore formation

The initial preparation of the acid at the beginning of the anodization produces a very strong acid with its conjugate base. Further addition of the base to the acid result in more deprotonation of the acid and either of the below is likely to occur for pH 3.5 with a weak acid being formed with its conjugate base.



Electro polishing flattens some large surface irregularities, but also creates a large number of small pores. Some of these pits can develop into pore nuclei.

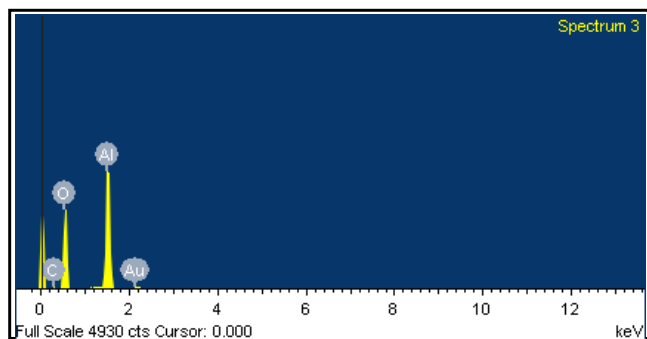
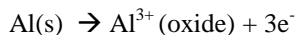
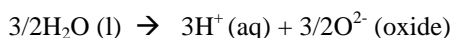


Fig. 2. EDAX spectra of pure samples as prepared Al₂O₃ films.

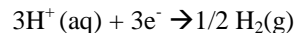
Their density will decrease as pores grow, because pores merge as anodizing time increases. Al³⁺ ions form at the metal/oxide interface and migrate into the oxide layer.



At the oxide/electrolyte interface the water-splitting reaction occurs and is rate-determining.



The O²⁻ (oxide) ions migrate, within the oxide from the oxide/solution interface toward the metal/oxide interface, to form Al₂O₃. Hydronium ions can also migrate toward the cathode, where they leave the electrolysis cell as H₂ gas, completing the circuit.



As anodization starts, the electric field at the oxide/electrolyte interface should be greater at sites where the native oxide coverage is thinner, or else the metal/oxide interface flattens out initially, so that the oxide layer is thicker in some parts of the surface, allowing the electric field to concentrate where the oxide is thinner.

Once small pores have formed, the acid and electric potential penetrate into the pore and the growth becomes self-catalyzing. Nanopores in aluminum oxidized in strong acids can become ordered either at certain voltages and times of the initial electro polishing or by long-term anodization and reanodization. **Fig. 1** shows the formation of larger pores. Unfilled circles are the pores formed at shorter time, whereas pores diameter increased as anodizing time increases, which are shown as filled circles. **Fig. 2** shows the EDAX spectrum of Al₂O₃ films.

The pattern shows the presence of only aluminium and oxygen and hence indicates the purity of Al₂O₃ films. The carbon peak which appeared in the spectra is due to the carbon tape pasted on copper grids used for the measurement. Au because of gold sputtering for conducting on Al₂O₃ films. **Fig. 3E** shows change in concentration (4%) at constant temperature, time and voltage.

As concentration decreases (**Fig. 3E**) the pore diameter decreases and wall thickness increases compare to **Fig. 3C**. If the temperature increases (**Fig. 3F**) the pore diameter increases and wall thickness decreases. It is observed that, the nanopores depend on concentration, temperature and time to grow different size nanopillars, which is tabulated in **Table 1**.

Table 1. Content of the pore diameter wall thickness and porosity of all the samples.

S. No.	Concentration H ₃ PO ₄ v/v%	Time min	Temperature °C	Voltage V	Wall Thickness nm	Average Pore Sizes nm	Porosity (α)%
A	5	5	20	50	58	32	0.2760
B	5	9	20	50	56	54	0.8438
C	5	20	20	50	48	58	1.3250
D	5	30	20	50	26	81	8.8078
E	4	20	20	50	52	55	1.0152
F	5	20	25	50	58	83	1.8584

Structural studies

The morphology of the anodized Al₂O₃ films was examined by field emission scanning electron microscopy (FESEM). **Fig. 3** shows the FE-SEM images of the anodized alumina structure. The anodization treatment of the templates in an acidic electrolyte. When Al is anodized in an acid (H₃PO₄), deep pores can form, with diameters varying between 32–81 nm (**Fig. 3** and **Table 1**). **Fig. 3 (A)** and **(B)** under a 50V applied potential shows the randomly distributed nano pores distributed all over the surface of the template because of the one step anodization process. The FE-SEM micrographs of the nanopores formed after 5% phosphoric

acid treatment at 5 to 30 min shows an increase in the diameter of the pores. The pores formed were observed to be well distributed all over the surface of the template (Fig. 3 (C) and (D)) compare to Fig. 3 (A) and (B), respectively. The effect of anodizing time on pore size and wall thickness is tabulated in the Table 1.

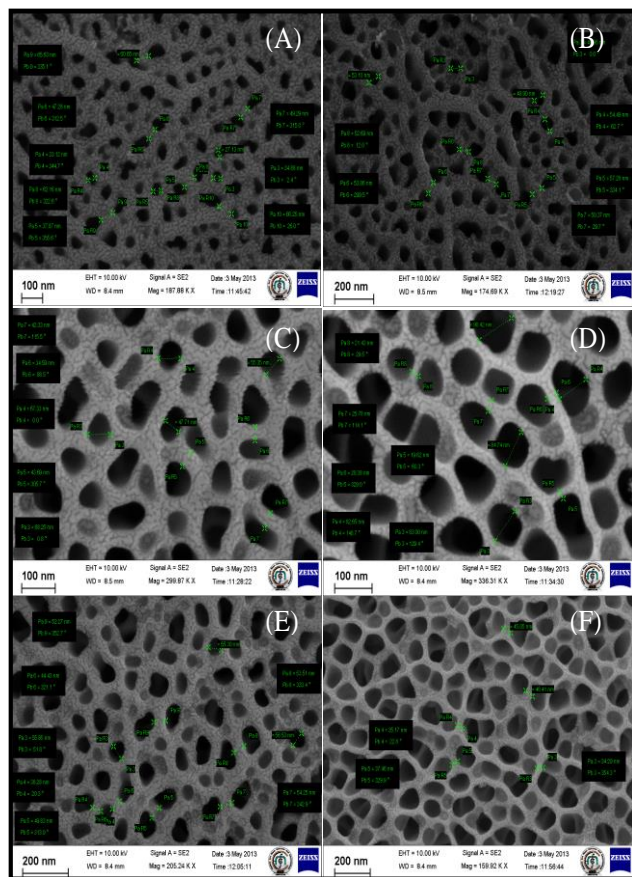


Fig. 3. FE-SEM images of the top view of anodized Al_2O_3 films at different time intervals (A) 5 min, (B) 9 min, (C) 20 min and (D) 30 min (E) Change in concentration (4%) at temperature, voltage at 20min and (F) change in temperature (25°C) at constant concentration, time and voltage.

The entire FE-SEM image shows the effect of increased anodizing time on the Al substrate, the pore diameter increases and wall thickness decreases, but the pore density decreases. Pore growth nucleation formation due to field-assisted hydrogen ion attack on the oxide layer. If the hydrogen ion concentration is decreased, then this attack will be slow. So the hydrogen ion attack must be fundamental to pores nucleation and development. The pore-type anodic aluminum oxide film grows in acidic solution, due to an electric-field-assisted local chemical dissolution at the oxide/electrolyte interface. It has been suggested that, at the bottom of the pores, the pH drops precipitously, increasing the solubility of the oxide; this is an “autocatalytic mechanism of pit propagation”. The nucleation and growth of this nonporous indicates that diameter and distances between neighbouring pores are highly uniform at constant temperature and voltage (Fig. 3). As the anodization time increases the pore diameter begin to grow. The results show that the regularity of the

naopores arrangement can be significantly improved by increasing anodizing time at constant concentration, temperature and voltage. With further decrease in concentration (Fig. 3E) reduces the pore diameter and increases the interpore distance compare to Fig. 3C. Surprisingly, increase in anodizing temperature indicates an increase in both pore diameter and interpore distance (Fig. 3F) compare to Fig. 3C. It can be attributed to the fact that the increase in anodizing time, concentration and temperature significantly changes the pores diameter and affects strongly their size uniformity. The average pore diameter and interpore distance were calculated from FE-SEM images. The bottom of each pore also consists of a thin “barrier layer” (30-100 nm thick) over the metallic Al surface; the pore diameter depends on pH, anodization voltage, and choice of acid. In contrast, at the other positions in the oxides-which contrary to region near the pore base already had been exposed to the electrolyte - different pore diameters were observed as a function of the position in the film as well as a function of the anodizing time. For all the considered anodizing time the pore diameter increased towards the oxide surface leading to pores. Since the oxide formation process occurs at the regressing metal-oxide interface, the oxide at the surface being most recently formed, i.e. near the pore base, the described phenomenon of pore widening increases with increasing time of exposure to the electrolyte and its dissolving action. This pores structure has been called “pore-type film” or “alumite the pore-type alumina films can be grown by anodizing Al TLC films at constant voltage. For growing the films with a desired pore diameter, the constant voltage mode is usually employed. The effect of enhanced oxide dissolution with increasing anodizing time that leads to a more porous oxide structure near the surface was considered quantitatively through the determination of the porosity by image analysis (Fig. 4). The porosity of the nanostructure formed by anodization of aluminium, defined as follows:

$$\alpha = \frac{\pi}{2\sqrt{3}} \left(\frac{D_p}{D_i} \right)^2$$

where, α is the porosity, D_p the pore diameter and D_i is the interpore distance. The increase in porosity of the structure with increasing anodizing time was observed at constant temperature and voltage (Fig. 3). As the Anodizing time increases the pore depth also increased, which is shown in Fig. 6. It has been suggested that, at the bottom of the pores, the pH drops precipitously.

Image analysis

The aim of the present study is to develop an automated method to determine the average growth size of the nanopores Al_2O_3 films, based on their geometric and statistical shape features. Many geometric and statistical features have been used by various authors in the literature [32-35]. It is observed that there are five geometric features, namely, length, width, area, box area ratio (BAR) and perimeter, which provide better results. Hence, we have used these five features, which are defined as given below:

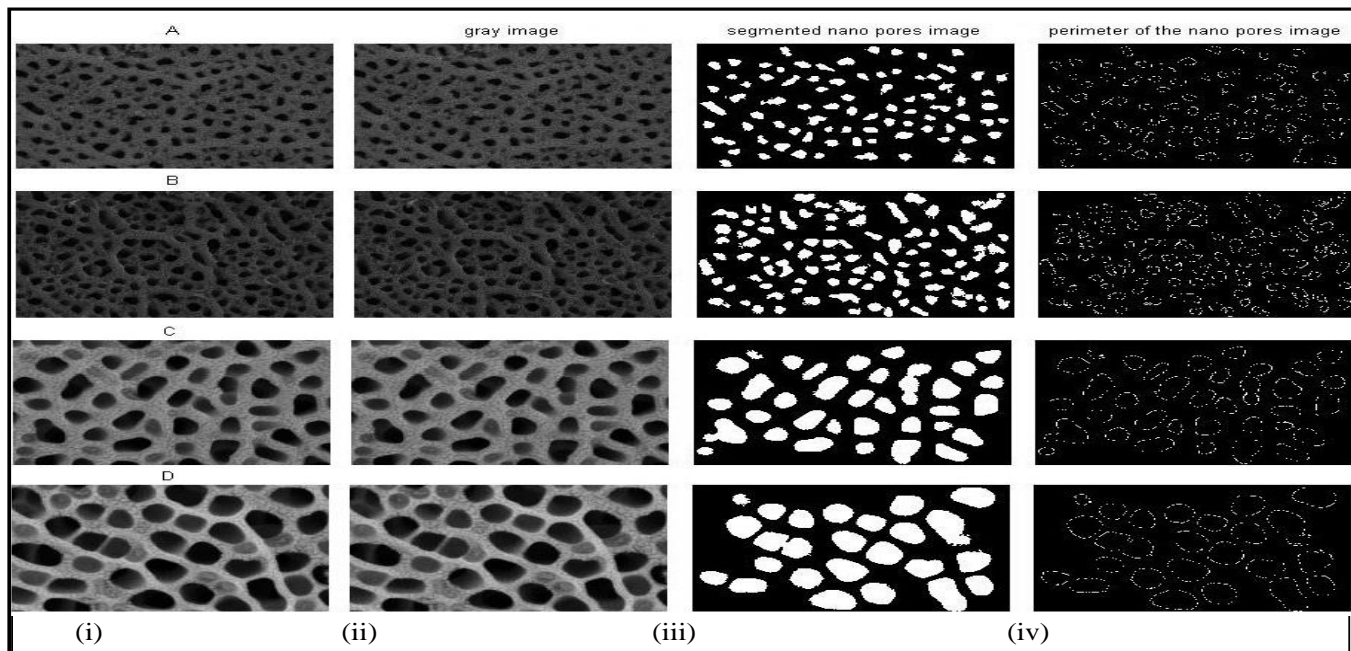


Fig. 4. (i) Original FE-SEM images at different times A-D, (iv) Perimeter image on (i)

Length: The longer side of smallest circumscribed rectangle.

Width: The shorter side of smallest circumscribed rectangle

Area: The number of pixels belonging to the object provides a measure of the object size.

Box Area Ratio (BAR): $\text{Length} \times \text{Width} / \text{Area}$ – The area of the smallest rectangle that can be drawn around an object, divided by the area of the object.

Perimeter: The grain boundaries of the pores.

The MATLAB algorithm for segmentation and feature extraction of nanopore regions in FE-SEM images is given as supporting data separately.

Image analysis results

The implementation is done on a Pentium Intel Core i3 @ 2.83 GHz machine using MATLAB 7.9. Each input FE-SEM image of nanopores image (Fig. 4(i)) is converted into grey scale image and the morphological operations such as erosion, reconstruction and dilation are functionalized. The resulting image was threshold to obtain

segmented binary image and obtained the perimeter of the nanopores are shown in Fig. 4(iv). The segmented image is labelled and for each segmented region (known pores) the geometric and statistical features are computed (Fig. 4 and Fig. 5).

Table 2. Geometric feature values of nanopore images of Fig. 3.

Samples	%	T	T°	V	Geometric feature values of nanopore images of Fig. 3				
					Length (x-size)	Width (y-size)	Box area ratio	Area	Perimeter
A	5	5	20	50	28.91	25.65	1.6385	450.57	114.1707
B	5	9	20	50	31.31	31.62	1.6957	590.01	143.2135
C	5	20	20	50	52	54.91	1.5087	1957.67	231.2353
D	5	30	20	50	71.29	68.41	1.4360	3467.04	301.9583
Geometric feature values of nanopore images of Fig. 4 with change in concentration (%) and temperature (T) at constant time and voltage (V)									
E	4	20	20	50	32.2469	35.086	1.4519	807.01	142.5062
F	5	20	25	50	37.7767	33.437	1.4118	907.13	144.4196

Table 2 represents the minimum and maximum geometric feature values computed for the segmented nanopore regions at different combination of concentration-time-temperature-voltage i.e., 5-5-20-50, 5-9-20-50, 5-20-

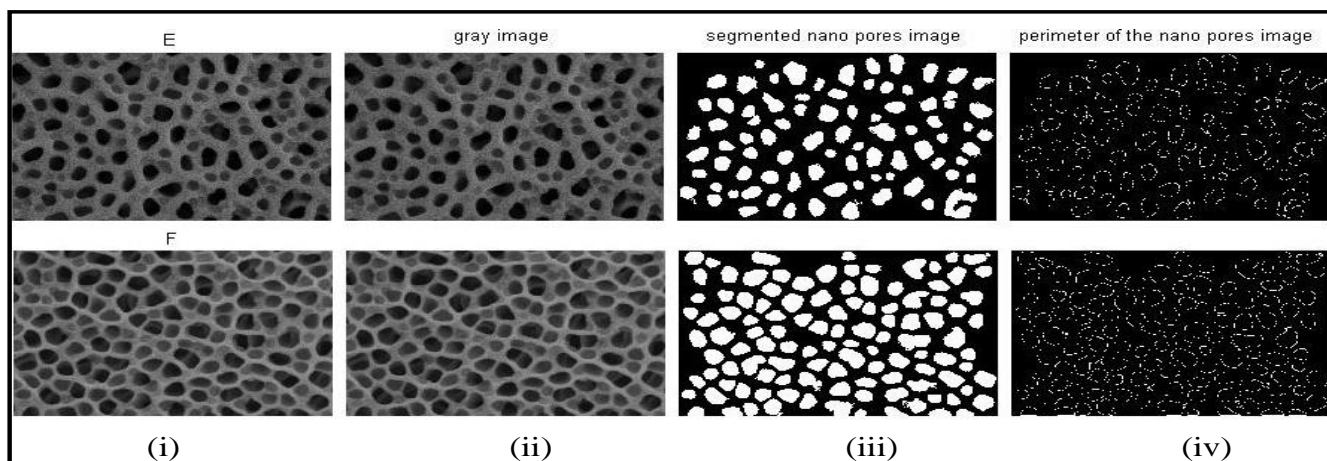


Fig. 5. (i) Original FE-SEM images at different times E-F, (iv) Perimeter image on (i)

20-50, 5-30-20-50, 4-20-20-50 and 5-20-25-50.

Fig. 7 shows with increasing anodizing time an increasing porosity and diameter at the surface of the (anodizing aluminium oxide) AAO was plotted. This inclining evolution became more pronounced for the increasing time, leading to an increase in porosity. The type of electrolyte, time and temperature of the electrolyte solution can affect the pore size and pore distribution of anodic alumina.

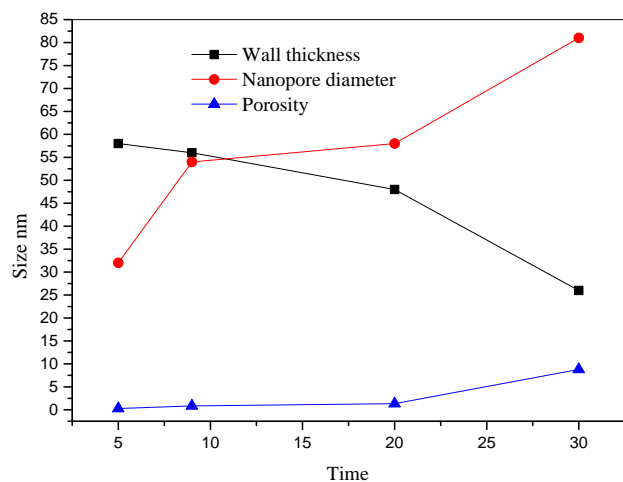
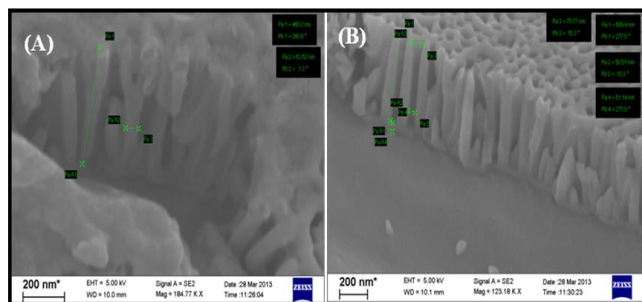


Fig. 6. FE-SEM images of the cross section of anodized Al_2O_3 films (A) Anodized aluminium sample A (B) Anodized aluminium sample D.

Fig. 7. Shows the effect of anodizing time on pore diameter and wall thickness of the Al_2O_3 films.

Conclusion

In conclusion, the time influence on the regularity of nanostructure formed by self-organised anodization of TLC aluminium in a 5 % phosphoric acid was analyzed. It is found that the regularity of nanopores arrangement can be significantly improved by increasing anodizing time at constant temperature and voltage. In the range of anodizing time from 9-30 min, the best uniformity obtained by anodization at 30 min. According to Nielsch, self-ordering of porous alumina requires a porosity of 10 % independently of anodizing conditions. It means that the most optimum anodizing conditions always results in a porosity of 10 %. The result optimized at 30 min is well matched with 10 % porosity. As increase in anodizing time significantly the rate of chemical dissolution and pore formation proceed rapidly. The pore diameters were found to be dependent on the time. As increasing anodizing time

results in increase in pore diameter, decrease in wall thickness and porosity of pure Al_2O_3 films. The average domain sizes are a linear function of time. The experimental results are compared with the automated computational results obtained by expert. The proposed method is computationally less expensive and yet yields comparable classification rates.

Acknowledgements

The authors gratefully acknowledge Indian institute of science (IISc), Bangalore for providing FE-SEM images. The authors thank to Vision Group of Science and technology (VGST), Govt. of Karnataka for the financial support.

Reference

- Rehan, K.; Zhiyong, F.; Kuniharu, T.; Javey, A. *Nano. Energ.* **2011**, *12*, 132.
- C. C. Vidyasagar, Y. Arthoba Naik, T. G. Venkatesh, R. Viswanatha, *Powder Tech.*, **2011**, *214*, 337.
- Hochbaum, A. I.; Yang, P. *Chem. Rev.* **2010**, *110*, 527.
- Tian, B.; Kempa, T. J.; Lieber, C. M. *Chem. Soc. Rev.* **2009**, *38*, 16.
- Patolsky, F.; Lieber, C. M. *Mater. Today*, **2005**, *8*, 20.
- Law, M.; Goldberger, J.; Yang, P. *Annual Rev. Mater. Res.* **2004**, *34*, 83.
- Kapadia, R.; Fan, Z.; Javey, A. *Appl. Phys. Lett.* **2010**, *96*, 103116.
- Kayes, B. M.; Atwater, H. A.; Lewis, N. S. *J. Appl. Phys.* **2005**, *97*, 1901835.
- Catchpole, K. R.; Mokkaapati, S.; Beck, F. J. *J. Appl. Phys.* **2011**, *109*, 084519.
- Kelzenberg, M. D.; Turner-Evans, D. B.; Kayes, B. M.; Filler, M. A.; Putnam, M. C.; Lewis, N. S.; Atwater, H. A. *Nano Lett.* **2008**, *8*, 710.
- Putnam, M. C.; Turner-Evans, D. B.; Kelzenberg, M. D.; Boettcher, S. W.; Lewis, N. S.; Atwater, H. A. *Appl. Phys. Lett.* **2009**, *95*, 163116.
- Tsakalagos, L.; Balch, J.; Fronheiser, B. A. Korevaar, O. Sulima J. Rand, J. Fronheiser, B. A. Korevaar, O. Sulima J. Rand, *Appl. Phys. Lett.* **2007**, *91*, 233117.
- Putnam, M. C.; Boettcher, S. W.; Kelzenberg, M. D.; Turner-Evans, D. B.; Spurgeon, J. M.; Warren, E. L.; Briggs, R. M.; Lewis, N. S.; Atwater, H. A. *Energy Environ. Sci.* **2010**, *3*, 1037.
- Zhong, Z. H.; Qian, F.; Wang, D. L.; Lieber, C. M. *Nano Lett.* **2003**, *3*, 343.
- Qian, F.; Gratecak, S.; Li, Y.; Wen, C. Y.; Lieber, C. M. *Nano Lett.* **2005**, *5*, 2287.
- Fan, Z. Y.; Wang, D. W.; Chang, P. C.; Tseng, W. Y.; Lu, J. G. *Appl. Phys. Lett.* **2004**, *85*, 5923.
- Hochbaum, A. I.; Chen, R. K.; Delgado, R. D.; Liang, E. C.; Garnett, W. J.; Najarian, M.; Majumdar, A.; Yang, P. D. *Nature* **2008**, *451*, 163.
- Wang, Z. L.; Song, J. H. *Science* **2006**, *312*, 242.
- Fan, Z. Y.; Razavi, H.; Do, J. W.; Moriwaki, A.; Ergen, O.; Chueh, Y. L.; Leu, P. W.; Ho, J. C.; Takahashi, T.; Reichertz, L. A.; Neale, S.; Yu, K.; Wu, M.; Ager, J. W.; Javey, A. *Nature Mater.* **2009**, *8*, 648.
- Stiebig, H.; Senoussaoui, N.; Zahren, C.; Haase, C.; Muller, J. *Photovoltaics*, **2006**, *14*, 13.
- Chin-Hung, L.; Szu-Ying, C.; Cheng-Ying, C.; Jr-Hau, H.; Lih-Juann, C.; Johnny, C. H.; Yu-Lun C. *ACS Nano*, **2011**, *5*, 6637.
- Masuda, H.; Fukuda, K. *Science* **1995**, *268*, 1466.
- Banerjee, P.; Perez, I.; Henn-Lecordier, L.; Lee, S. B.; Rubloff, G. W. *Nat. Nanotechnol.* **2009**, *4*, 292.
- Liang, Y.; Schwab, M. G.; Zhi, L.; Mugnaioli, E.; Kolb, U.; Feng, X.; Meullen, K. J. *Am. Chem. Soc.* **2010**, *132*, 15030.
- Min Hyung, L.; Namsoo, L.; Daniel Ruebusch, J.; Jamshidi, A.; Kapadia, R.; Lee, R.; Joon Seok, T.; Takei, K.; Young Cho, K.; Fan, Z.; Jang, H.; Wu, M.; Cho, G.; Javey, A. *Nano Lett.* **2011**, *11*, 3425.
- Kumar, G.; Tang, H. X.; Schroers, J. *Nature*, **2009**, *457*, 868.
- Lyvers, D. P.; Moon, J. M.; Kildishev, A. V.; Shalaev, V. M.; Wei, A. *ACS Nano*, **2008**, *2*, 2569.
- Vlassioulak, I.; Krasnoslobodtsev, A.; Smirnov, S.; Germann, M. *Langmuir* **2004**, *20*, 9913.
- Diggle, J. W.; Downie, T. C.; Goulding, C. W. *Chem. Rev.* **1969**, *69*, 365.

30. Feiyue, L.; Zhang, R.; Metzger, M. *Chem. Mater.* 1998, 10, 2470.
31. Shwetabh, S. *J. Computer Eng.* **2013**, 11, 84.
32. Fisker, R.; Carstensen, J. M.; Hanshen, M. F.; Bodker, F.; Morup, S. *J. Nanoparticle Res.* **2000**, 2, 267.
33. Rafael, C. G.; Richard, E. W. *Digital Image Processing*, Pearson Education Asia, **2002**.
34. John, C. R.; *The Image Processing Hand Book* **2007**, 5th Ed. CRC Press, New Jersey.
35. Micheli-Tzanakou, E. *Feature Extraction and Computational Intelligence* CRC Press LLC, Florida **2000**.

Advanced Materials Letters

Copyright © 2016 VBRI Press AB, Sweden
www.vbripress.com/aml and www.amlett.com

Publish your article in this journal

Advanced Materials Letters is an official international journal of International Association of Advanced Materials (IAAM, www.iaamonline.org) published monthly by VBRI Press AB from Sweden. The journal is intended to provide high-quality peer-review articles in the fascinating field of materials science and technology particularly in the area of structure, synthesis and processing, characterisation, advanced-state properties and applications of materials. All published articles are indexed in various databases and are available download for free. The manuscript management system is completely electronic and has fast and fair peer-review process. The journal includes review article, research article, notes, letter to editor and short communications.



VBRI Press

a rapid publication platform

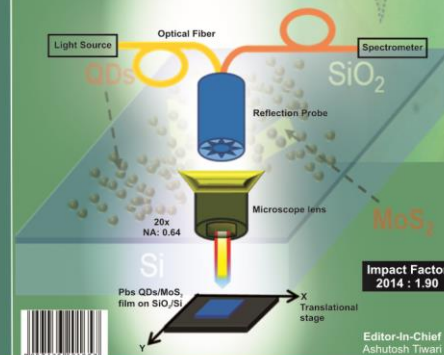
**A
Monthly
Journal**

November 2015

ISSN 0976-3961

Advanced Materials Letters

Structure: synthesis & processing, characterization, advanced-state properties and application of materials



An official journal of International Association of Advanced Materials, www.iaamonline.org

JOURNAL
VBRI Press

Editor-in-Chief
 Ashutosh Tiwari

Available online at
www.amlett.com and www.vbripress.com/aml